Japanese Journal of Applied Physics **53**, 07KF08 (2014) **REGULAR PAPER**
http://dx.doi.org/10.7567/JJAP.53.07KF08

Echo speckle imaging of blood particles with high-frame-rate echocardiography

Hiroki Takahashi[1]*, Hideyuki Hasegawa[1,2], and Hiroshi Kanai[1,2]

[1]*Graduate School of Biomedical Engineering, Tohoku University, Sendai 980-8579, Japan*
[2]*Graduate School of Engineering, Tohoku University, Sendai 980-8579, Japan*
E-mail: htaka@us.ecei.tohoku.ac.jp

Received November 26, 2013; revised February 21, 2014; accepted March 5, 2014; published online June 13, 2014

Cardiac blood flow patterns such as the vortex flow pattern inside the left ventricle have been studied to provide new information for the diagnosis of the pumping function of the human heart. Complex blood flow is visualized by imaging echo speckles of blood particles because the speckle-like texture translates to the motion of blood particles. We proposed an imaging method for echo speckles of blood particles using high-frame-rate ultrasound for the visualization of the intracardiac blood flow direction. High-frame-rate ultrasound is useful for continuously observing the fast motion of echoes from blood particles in the heart. In the present study, weighting by coherence and compounding the magnitudes of echo signals in different transmissions were introduced to visualize weak echoes from blood particles. The feasibility of the visualization of cardiac blood flow using high-frame-rate ultrasound was demonstrated by basic and in vivo experiments.

1. Introduction

Echocardiography is a predominant imaging modality for the evaluation of the cardiac function because it could provide a cross-sectional image of the heart noninvasively in real time. Recently, it has been shown that the ultrasonic measurement of myocardial contraction and its propagation is useful for the evaluation of the myocardial function.[1–3] On the other hand, the evaluation of blood flow structures in echocardiography is also useful for the diagnosis of the pumping function of the human heart.[4,5] As a typical method, color Doppler flow imaging (CDI) has been widely used to obtain information on intracardiac blood flow in clinical practice. CDI, however, does not show the direction of blood flow because it provides only the velocity component along an ultrasonic beam. Recently, cardiac blood flow patterns such like the vortex flow pattern in left ventricular cavity have been studied to provide new information for diagnosis by contrast echocardiography, which is called echocardiographic particle image velocimetry (E-PIV).[6–8] E-PIV gives the distribution of velocity vectors of blood flow, which is calculated on the basis of the motion of ultrasonic echoes from contrast agents. E-PIV, however, creates physical and mental burden in patients owing to the intravenous injection of a contrast agent.

An estimator of the velocity vector of blood flow has been developed by several researchers. Tortoli and coworkers[9,10] proposed a method of determining the angle of blood flow, where a beam is used for estimating the flow direction by identifying the angle that shows symmetrical Doppler spectra with respect to the zero frequency. Another beam is used to obtain the angle-corrected Doppler spectra. Jensen and Nikolov[11] developed a method of flow vector estimation using a synthetic aperture technique. In their method, echo signals are created along the manually determined flow direction and the flow velocity magnitude is estimated by applying a cross-correlation technique to echoes obtained by those beams. These methods are intended for the measurement of blood flow inside a vessel where blood particles move on a preassigned streamline along the blood vessel. However, the blood flow inside the cavity of the heart exhibits complex flow patterns, such as a vortex pattern, in contrast to the vascular flow. Furthermore, blood particles flow at a velocity of over 1 m/s in the human heart. Hence, a method of scanning a broad region that covers the ventricular cavity in a short time, i.e., high-frame-rate imaging, is required to visualize the complex and fast flux in the human heart. High-frame-rate ultrasound with parallel beamforming,[12,13] therefore, would be of value for the visualization of a rapid and complex blood flow. Some authors have suggested methods of visualizing the direction of blood flow in a blood vessel by analyzing the motion of echoes from blood particles using parallel beamforming with plane wave transmission.[14–16] Moreover, the intracardiac vector flow of neonates and children was visualized by high-frame-rate ultrasound with plane wave transmission using a linear array probe.[17] However, a phased array probe is normally used for the sector scanning of an ultrasound beam in cardiac ultrasound. The use of plane waves, hence, limits the scan speed in cardiac ultrasound because the width of insonified plane waves does not increase with the range distance from the probe in a near field, whereas the lateral interval of scan lines increases with the range distance, and the width of plane waves decreases with an increase in the steering angle.

Hasegawa and Kanai developed an alternative method of high-frame-rate echocardiography using parallel beamforming with spherically diverging waves emitted with all transducer elements.[18,19] These spherical diverging waves used in this method do not limit the illuminated region by the size of the aperture and enable the acquisition of echoes with higher signal-to-noise ratios (SNRs) than the synthetic aperture ultrasound,[11,20] which uses one or small number of elements.

We proposed a method for the visualization of the intracardiac blood flow direction using parallel beamforming with the transmission of spherically diverging waves. Coded excitation was used to enhance weak echoes from blood particles. Echoes from blood particles were extracted using high-pass filtering for clutter suppression. In addition to these conventional techniques, two unique approaches were proposed to enhance echoes from blood particles in the proposed method. To suppress undesired noise components in the filtered echo signals, high-pass filtered echo signals were weighted using a coherence function in the first approach. Compounding was applied between transmissions to envelope signals in the second approach because echo signals from moving blood particles obtained in different transmissions cancel each other when compounding is

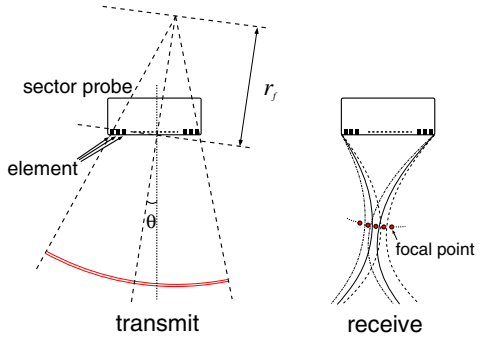

Fig. 1. (Color online) Illustration of transmission of spherically diverging beam and parallel receive beamforming using phased-array probe.

applied to RF signals. The accuracy of our proposed method was evaluated by a basic experiment using blood-mimicking fluid flowing inside a tube. Furthermore, the feasibility of the proposed method was demonstrated by an in vivo experiment.

2. Principles

2.1 Parallel receive beamforming with spherically diverging wave for high frame rate echocardiography

In this study, parallel receive beamforming with spherically diverging beams (PBF-DB), which is shown in Fig. 1, was used. Using PBF with broad transmit beams, echo signals are measured at a high frame rate without sacrificing the density of scan lines. A spherically diverging wave, which can illuminate a wider region, was transmitted to solve the problem of the limited width of a plane wave. An ultrasonic image of a blood pool, which is filled with blood particles (scatterers), has a speckle-like texture[21,22] because the constructive and destructive interferences among echoes from many scatterers much smaller than the wavelength of transmitted ultrasound occur in the focal point, as shown in Fig. 2. Thus far, many researchers have examined methods utilizing an echo speckle, which contains information on tissue structures for blood flow vector estimation,[23] the quantitative evaluation of liver fibrosis,[22,24] and shear wave velocity measurement for tissue elasticity imaging.[25–27] An echo speckle, which arises from blood echoes, translates between successive frames, i.e., the spatial feature of an echo speckle is preserved, when blood particles move in the same direction without changing their relative distance. The velocity vector of a slow blood flow in the left atrium has been calculated using the dynamic texture produced by strong backscattering.[28] However, the speckle texture frequently transmutes during a short time because blood particles in the left ventricular cavity flow at a velocity of up to 1 m/s. PBF-DB is helpful for preserving the spatial feature of echo speckles during a frame interval because the frame rate is further increased by imaging a wider region by one transmission as compared with parallel beamforming with plane wave transmission. In Fig. 1, r_f and θ are the distance from a virtual point source behind the array to the center of the transducer array and the steering angle, respectively. A spherically diverging beam is formed by activating each transducer element with a time delay calculated using r_f and θ.[18,19]

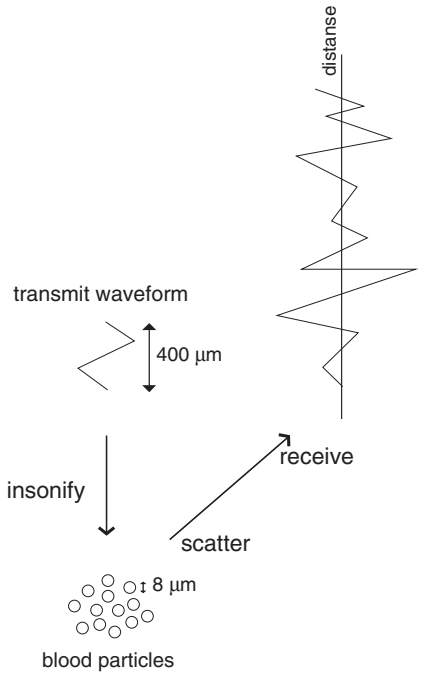

Fig. 2. Illustration of echo waveform from region composed of many blood particles, i.e., many scatterers much smaller than the wavelength at an ultrasonic frequency of 3.75 MHz. Echo signals from blood particles are indistinguishable from each other owing to the interference of the scattered signals.

2.2 Coded excitation for enhancement of echoes from blood particles

The amplitude of a scattered signal depends on the size of the scatterer, the reflection coefficient of the surface of the scatterer, and the frequency of the transmitted ultrasound.[29] Most of the blood particles are red blood cells, which are very small ultrasonic scatterers whose diameter is almost 8 μm. The reflection coefficient between the blood particle and blood plasma is also small.[30] It is well known that the power of echoes from scatterers like red blood cells is proportional to the fourth power of frequency. It is, however, necessary to transmit low-frequency ultrasound waves (from 2 to 5 MHz) in cardiac ultrasound to get echoes with better SNRs from the profound heart by avoiding significant frequency-dependent attenuation. Hence, the enhancement of echo signals from blood particles is essential for the visualization of echo speckles of blood particles in cardiac ultrasound. SNRs of echo signals from blood particles can be increased by temporal (frame) averaging. Temporal averaging, however, degrades the spatial features of echoes from blood particles because echo speckles of blood particles are blurred owing to the motion of blood particles during temporal averaging. On the other hand, the SNRs of echo signals could be improved by increasing the transmit pulse amplitude, but the transmit pulse amplitude is limited by safety regulations. Bi-phase-coding, such as Barker and Golay coding, which improves the SNRs of signals by the compression of longer pulses without safety violations, could be realized at a low cost.[31] Since Golay coding requires two transmissions, the compression gain would be further degraded by the tissue motion between two transmissions. Hence, in the present study, coded excitation and pulse compression with a Barker code,[32] which is a single-transmit code, were used to

increase the SNRs of weak echoes from blood particles. The excitation signal was coded with a 13-bit Barker code. Moreover, the echo signal received at each element was individually decoded before receive beamforming.

2.3 High-pass filtering for clutter suppression

Echoes from stationary and slowly moving tissues such as the ribcage and myocardium caused by the sidelobe, which are called clutter signals, contaminate those from blood particles in the cardiac lumen. Suppressing the clutter noise is essential for extracting echoes from blood particles because the amplitudes of clutter echoes are usually much larger than those of echoes from blood particles. On the other hand, the motion velocity of the myocardium is different from that of blood particles. The maximal velocity of the myocardium is almost 0.1 m/s, whereas that of blood flow in the human heart reaches to 1 m/s. Clutter signals, hence, have a lower-Doppler-frequency component than echo signals from blood particles, which corresponds to a small change in the phase of an echo signal in the direction of the frame. In the present study, clutter signals were suppressed by high-pass filtering in the direction of the frame. The filters' impulse response was the sinc function multiplied by the Kaiser window, which is linear time-invariant. Myocardial walls normally move with a velocity of up to 0.1 m/s,[33] which corresponds to a Doppler frequency of 500 Hz in the case of a transmission frequency of 3.75 MHz. To suppress clutter signals generated by sidelobes, the cutoff frequency of a clutter filter was set to 500 Hz.

2.4 Weighting by coherence for noise suppression

The undesirable noise component, which is generated by electronic devices, still remains in the high-Doppler-frequency range although a clutter filter is used. The suppression of the remaining noise is efficient for the visualization of echoes from blood particles because the noise component contaminates weak echoes from blood particles.

The temporal changes in the phase of the signal component (corresponding to echoes from an object) would be spatially constant during a pulse duration, i.e., coherent. The temporal changes in the phase of the signal component at a certain depth is also assumed to be constant for a short period (small number of frames). On the other hand, the temporal changes in the phase of the noise component are random, spatially and temporally. Therefore, in the present study, the random noise remaining in the high-Doppler-frequency range was suppressed by weighting using the ratio of the coherent component to the total signal. The coherent component was obtained by minimizing the noise component using the least square method applied to quadrature demodulated signals. Let us define the complex demodulated signal at the frame number i and the sampled point number n, which corresponds to time $t = nT$ (T: sampling interval) as $x_i(n)$. The normalized mean square error (corresponding to the ratio of the noise component) α among complex RF signals $\{x_i(n)\}$ for a few sampled points N_d and frames N_f is expressed as follows:

$$\alpha = \frac{\mathrm{E}_k[\mathrm{E}_m[|x_{i+m}(n+k) - z \cdot x_{i+m-1}(n+k)|^2]]}{\mathrm{E}_k[\mathrm{E}_m[|x_{i+m}(n+k)|^2]]}, \quad (1)$$

where z, $\mathrm{E}_k[\cdot]$, and $\mathrm{E}_m[\cdot]$ denote the transfer function from $\{x_{i-1}(n)\}$ to $\{x_i(n)\}$ and the averaging procedures with respect to the depth and frame, respectively. The averaging numbers of $\mathrm{E}_k[\cdot]$ and $\mathrm{E}_m[\cdot]$ are defined by N_f and N_d, respectively. The estimated $\hat{z}$, which minimizes α, can be estimated by the least square method using Eq. (1). By substituting $\hat{z}$ into Eq. (1), the minimum mean square error $\alpha_{\min}$ is obtained as follows:

$$\alpha_{\min} = 1 - \frac{|\mathrm{E}_k[\mathrm{E}_m[x^*_{i+m-1}(n+k)x_{i+m}(n+k)]]|^2}{\mathrm{E}_k[\mathrm{E}_m[|x_{i+m-1}(n+k)|^2]]\mathrm{E}_k[\mathrm{E}_m[|x_{i+m}(n+k)|^2]]}. \quad (2)$$

The obtained $\alpha_{\min}$ corresponds to the normalized residual noise component in the signal $\{x_i(n)\}$, which cannot be predicted by $\{x_{i-1}(n)\}$. Hence, the instantaneous intensity of the coherent component at the n-th depth point in the i-th frame is obtained as $(1 - \alpha_{\min})$, and the estimate $\hat{S}_i(n)$ of the amplitude of echo from blood particles is obtained by weighting the instantaneous signal amplitude $|x_i(n)|$ with the coherency $\sqrt{1 - \alpha_{\min}}$ as follows:

$$\hat{S}_i(n) = |x_i(n)|\sqrt{(1 - \alpha_{\min})}. \quad (3)$$

In the present study, the lengths for averaging in the frame and depth directions, N_f and N_d, were set to 6 and 8 (corresponding to about 2 ms and 0.5 μs), respectively. The random noise contained in high-pass-filtered echo signals would be suppressed by weighting the echo amplitude with coherency.

2.5 Compounding of speckle images obtained by different transmissions

In PBF with a wide transmit beam for high-frame-rate echocardiography, discontinuities of echo intensities occur in an ultrasound image because the transmit–receive directivity significantly changes owing to the large interval between neighboring transmit beams. To solve this problem, compounding echo signals obtained by different transmissions is effective.[18] The compounding procedure, however, would not fit the visualization of echoes from blood particles because the phase of the echo signals from fast moving objects, such as blood particles, differs significantly among emissions and coherent compounding would be difficult.[11] Incoherent compounding weakens echoes from blood particles. In the present study, the envelope of high-pass-filtered RF signals in each transmission, which removes phase information, was compounded (summed) to avoid such compensation. Figure 3 shows a schematic diagram of the proposed method. Let us define this technique for blood echo speckle visualization "magnitude compounding". At first, clutter filtering and weighting by coherence were applied to beamformed RF signals obtained from each transmission. Then, from the filtered RF signals, the signal amplitudes [corresponding to $\hat{S}_i(n)$ in Eq. (3)] were extracted. Finally, the amplitudes $\{\hat{S}_i(n)\}$ obtained for multiple transmissions were compounded. The effect of magnitude compounding was verified in the subsequent section.

3. Materials and methods

A blood-mimicking fluid (Shelly Medical Imaging Technologies US model) that was made to flow through a cylindrical tube was measured by ultrasound. The internal and external diameters of the tube made of urethane rubber were 8 and 12 mm, respectively. The tube contained 5% carbon powder (by weight) to obtain sufficient scattering from the wall for

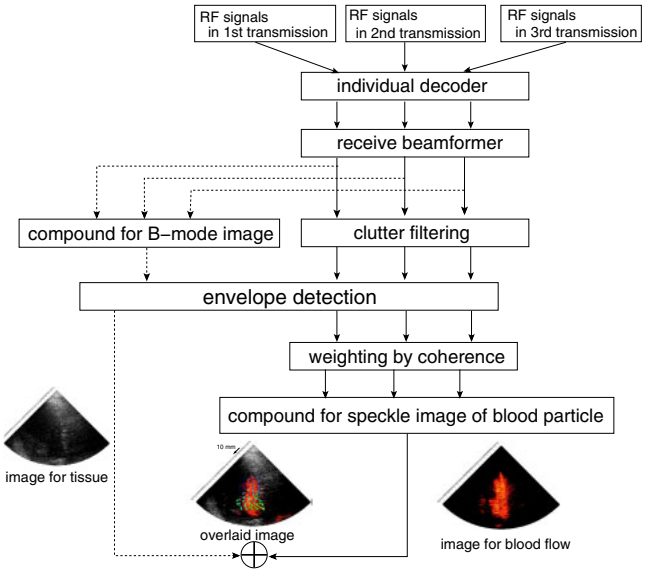

Fig. 3. (Color online) Schematic of procedure of proposed method of imaging of movement of echoes from blood particles.

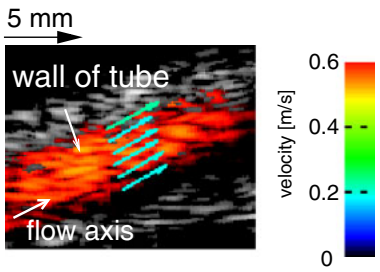

Fig. 4. (Color online) Echo speckles overlaid on B-mode image and velocity vector distribution along direction perpendicular to flow axis for estimation of flow rate of blood-mimicking fluid flowing inside tube.

Table I. Cross-sectional areas of lumen of tube.

Rotation rate of screw (min^{-1})	Cross-sectional area (cm^2)
160	0.56
260	0.53
360	0.44
460	0.38

the identification of the walls, between which the blood-mimicking fluid flowed. The blood-mimicking fluid was made to steadily flow using a screw pump (Heishin 2NL10PU), which could control the flow rate in proportion to the rotation rate of the screw. The Reynolds number reached up to 1070 under the present experimental conditions. To avoid to the generation of tiny air bubbles in the fluid flowing inside the tube, the blood-mimicking fluid was deaerated using a vacuum pump.

The tube and human heart were measured by a modified diagnostic ultrasound system (Hitachi-Aloka Medical Alpha 10) with a 3.75 MHz phased array probe. This system was modified to acquire individual RF echo signals, which were sampled at 15 MHz, received by 96 elements. The spherically diverging wave was transmitted in three directions and steered at -10, 0, and $+10°$. PBF and the proposed process for the visualization of blood flow were applied to off-line processing.

The velocity vector of the flow was estimated by applying the speckle tracking technique[23] to the distributions of echo amplitudes in two frames, which was obtained using Eq. (3). The velocity vector was obtained by searching for the maximum of the two-dimensional cross correlation function between the echo amplitudes inside kernels in two consecutive frames. The kernel sizes in the lateral and axial directions in the speckle tracking technique were set to 9° and 4.6 mm, respectively. Note that the cross correlation map was up-sampled[34] by factors of 120 and 10 in the lateral and axial directions, respectively, before calculating the cross correlation function.

4. Basic experimental result

The distance between the outer surface of the tube anterior wall and the probe surface was set at 5 cm. The angle between the probe surface and the tube was maintained at 15°. The tube's longitudinal direction (corresponding to the flow axis) was manually identified in the B-mode image. The velocity vectors of the fluid inside the tube were estimated at 0.5 mm intervals along the manually assigned line by applying the speckle tracking method to echo speckles from blood particles obtained by the proposed method. Figure 4 shows a B-mode image of the tube obtained by PBF-DB overlaid with blood echo speckles and the estimated velocity vectors. The components of the estimated flow vectors along the direction of the flow axis were averaged as follows:

$$Q = \frac{A}{N_j} \sum_{j=0}^{N_j-1} \boldsymbol{v}_j \cdot \boldsymbol{n}_f, \tag{4}$$

where A, $\boldsymbol{v}_j$, and $\boldsymbol{n}_f$ denote the cross-sectional area where the blood-mimicking fluid flowed, the estimated velocity vector of the j-th spatial point, and the unit vector parallel to the flow axis, respectively. The cross-sectional area of the lumen of the tube, A, was changed by the suction pressure of the pump depending on the rotation rate of the screw. Table I shows the cross-sectional area of the lumen of the tube measured in the short-axis view obtained with Alpha 10 by manually segmenting B-mode images to accurately estimate the flow rate.

The flow rate was estimated by a flow meter (Keyence FD-SF1) and our proposed method, while the rotation rate of the screw pump was varied as 160, 260, 360, and 460/min. The performance curve of the pump between the rotation rate of the screw and the flow rate was estimated on the basis of relationship between the rotation rate and the flow rate up to 1000 mL/min because the accuracy of the flow meter was not guaranteed when the flow rate was over 1000 mL/min of the flow rate. Figure 5 shows the flow rate plotted as a function of the rotation rate of the screw and the regression line estimated by the least square technique, which is given as $y = 3.4x - 9.2$ mL/min [y and x correspond to the flow rate (mL/min) and rotation rate of screw (/min), respectively]. Figure 6 shows the flow rate estimated by our proposed method with magnitude compounding (red crosses) and our proposed method with compounding of RF signals (green crosses). In Fig. 6, plots and vertical bars denote the means

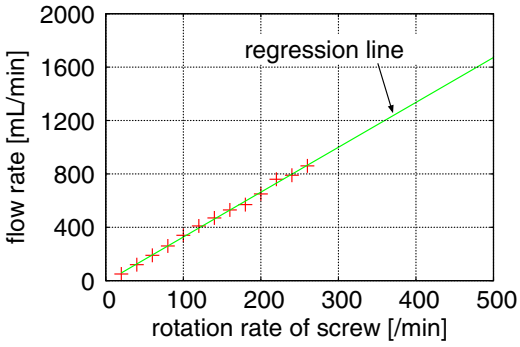

Fig. 5. (Color online) Flow rates measured at different rotation rates of screw and regression line estimated by least square technique. The regression line is given as $y = 3.4x - 9.2$ [mL] (y and x correspond to the flow rate [mL/min] and the rotation rate of the screw [/min], respectively).

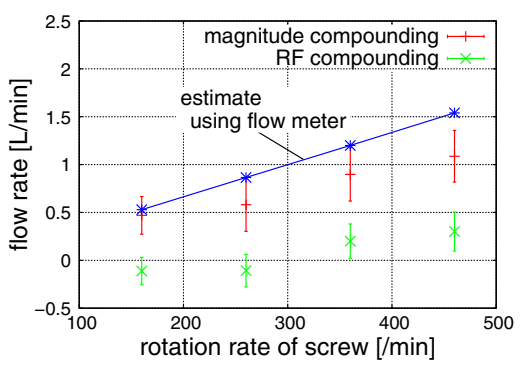

Fig. 6. (Color online) Flow rate of blood-mimicking fluid obtained using flow meter, proposed method with RF signal compounding, and proposed method with magnitude compounding.

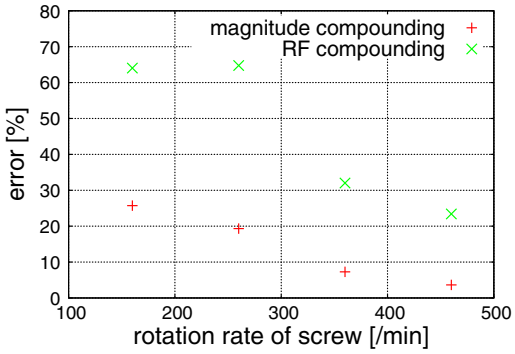

Fig. 7. (Color online) Error of direction of velocity vector estimated by proposed method with RF signal compounding and proposed method with magnitude compounding.

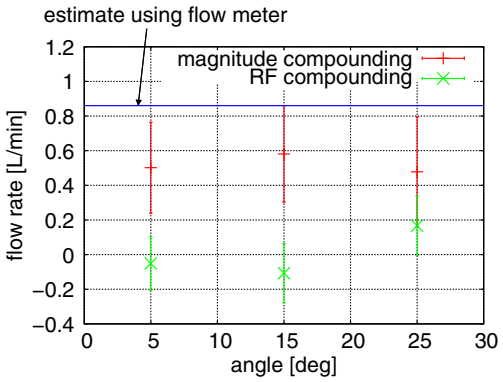

Fig. 8. (Color online) Means and standard deviations of flow rate estimated by proposed method at three different angles between the surface of probe and the tube: about 25, 15, and 5°.

and standard deviations of the flow rate in the temporal direction for 50 frames. As shown in Fig. 6, the difference between the means obtained using the proposed method and flow meter was reduced by magnitude compounding. From these results, the cancellation of RF signals caused by the movement of particles degraded the accuracy of the estimation of the velocity vector, and such degradation was suppressed by the proposed method. The proposed method, nevertheless, tended to underestimate the flow rate.

The mean error e_{dir} of the direction of the estimated flow vector was also evaluated using the following equations:

$$e_{\mathrm{dir}} = \frac{1}{N_i}\sum_{i=0}^{N_i}\frac{\sqrt{\mathrm{E}_j[(\arg(\boldsymbol{n}_f) - \arg(\boldsymbol{v}_{i,j}))^2]}}{\pi}, \qquad (5)$$

where E_j and $\arg(\cdot)$ represent the spatial averaging procedures with respect to the points of interest assigned along the direction perpendicular to the flow axis and the argument of a vector. Figure 7 shows the mean error of the direction of the flow vector, e_{dir}, estimated by the method proposed in this study plotted as a function of the rotation rate of the screw pump. As shown in Fig. 7, the use of the magnitude compound could significantly reduce the error in the estimated flow direction. Figure 8 shows the flow rate at a rotation rate of the screw of the 260/min, estimated at angles between the probe surface and the tube of 25, 15, and 5. The movement of echo speckles of blood particles could not be clearly seen at angles of over 25° because the transmitted ultrasound could not penetrate the tube well owing to the small insonification angle. The standard deviation of the estimated flow rate was high, but the means were not very different among the angles of 25, 15, and 5. From these results, the accuracy of the flow direction estimated by the proposed method was improved using magnitude compounding. In this basic experiment, the SNRs of echoes from particles mimicking blood particles were much higher than those from blood particles in the human heart because the ultrasonic attenuation of water was very low. A higher acoustic output, therefore, would be desired for better visualization of echo speckles of blood particles in in vivo transthoracic measurement. Furthermore, the velocity and direction of blood flow rapidly vary in the human heart. However, the blood-mimicking fluid steadily flowed in this basic experiment. Hence, the time length (number of frames) for clutter filtering, which was set to almost 13 ms in this study, should be as short as possible to suppress contamination by RF signals in other frames, which exhibit a blood velocity significantly different from that in the target frame.

5. In vivo experimental result

As shown in Fig. 9(a), ultrasonic RF echo signals from the left ventricle were measured in a three-chamber view of a 26-year-old healthy male at a very high frame rate of 2008 Hz. The healthy subject gave informed consent in the study.

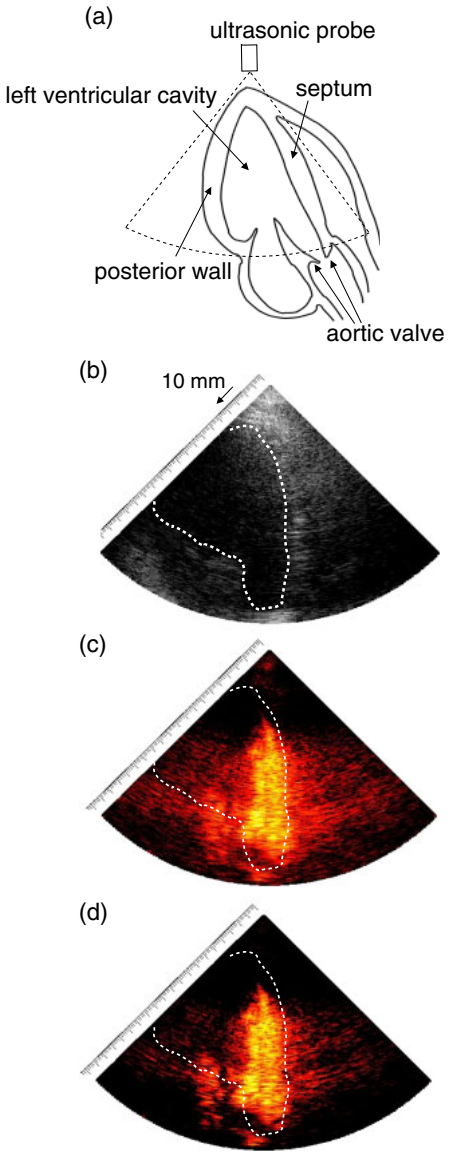

Fig. 9. (Color online) (a) Illustration of measurement region in three-chamber view and (b) B-mode image obtained by PBF-DB in a certain frame in systole. Speckle images of blood particles (c) without weighting and (d) with weighting by coherence. White dashed lines show the roughly estimated boundary of the left ventricular cavity.

Figure 9(b) shows the B-mode image obtained using PBF-DB in a frame in systole. Figures 9(c) and 9(d) show only speckle images of blood particles (shown on a hot scale) in the same frame obtained using the proposed method without and with weighting by coherence, respectively. The intensity was individually normalized by the maximums in Figs. 9(c) and 9(d) in that frame. As can be seen in Figs. 9(c) and 9(d), speckle-like patterns of echoes from blood particles were visualized inside the left ventricular cavity by suppressing echoes from the myocardium. Moreover, the noise components, which were seen like small and randomly distributed particles, were suppressed by weighting with coherence, as can be seen in the region surrounded by the white dashed line in Figs. 9(c) and 9(d).

Figures 10(a) and 10(b) show flow velocity vectors overlaid on the B-mode images in frames in systole and diastole, respectively. The motion of speckle-like patterns

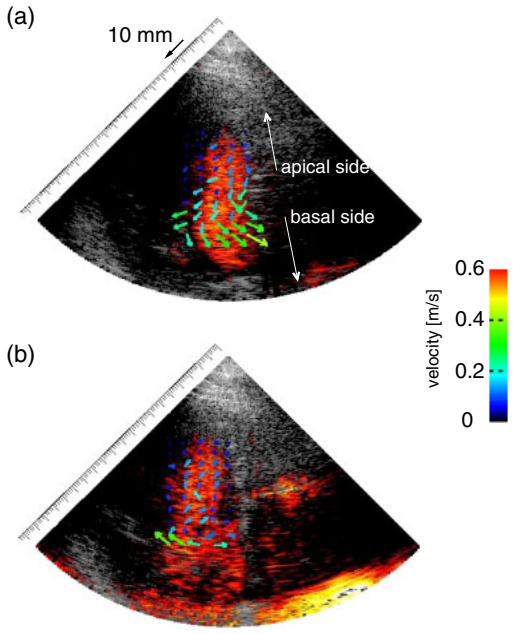

Fig. 10. (Color online) (a) B-mode image (shown by gray-scale) overlaid with speckle image of blood particles (shown by hot-scale) at frames in (a) systole and (b) diastole with flow velocity vectors estimated by the speckle tracking technique.

directed to the aortic valve showed that blood in the left ventricular cavity was ejected to the aorta in systole, as shown in Fig. 10(a). On the other hand, as shown in Fig. 10(b), speckles of blood particles move to the apex side from the basal side in diastole, which corresponds to blood flowing into the cavity.

6. Discussion

The accuracy of the estimation of the velocity vector was improved in terms of both flow rate (corresponding to flow velocity) and direction by magnitude compounding, as shown in Figs. 6 and 7, because SNRs of echoes from fast-moving blood particles were improved by avoiding the compensation caused when RF signals were compounded incoherently. The mean flow rates estimated using the proposed method, nevertheless, tended to be lower than those estimated using the flow meter, as shown in Fig. 6. Moreover, the diameter of the tube inhomogeneously changed in a circumferential direction with an increase in flow rate (particularly, at a rotation rate of over 360/min) because the elasticity of the wall of the custom-made tube was inhomogeneous. Therefore, the flow velocity estimated along the assigned line was considered to be different from the mean flow velocity averaged in the cross section of the tube. Moreover, in the experimental situation, turbulent flow was generated because the Poiseuille flow was not fully developed owing to an insufficient length of the inlet to the tube. On the other hand, the kernel size in the speckle tracking technique used in the present study, was $7.9 \times 4.6\,\mathrm{mm}^2$ at a depth of 5 cm, which was close to the inner diameter of the tube of 8 mm. The kernel, therefore, could not follow fast-moving particles because the movements of particles were not homogeneous owing to the flow-rate gradient of the Poiseuille flow and small regional turbulence. On the other hand, under the in vivo condition, it is also

difficult to estimate the velocity vectors of complex blood flow using a large kernel when blood particles in the kernel move inhomogeneously. A velocity vector estimator with a high spatial resolution is desired to visualize the vector distributions of complex blood flow in the cardiac cavity. To solve a such problem, the spatial resolution of the velocity vector estimator should be improved by considering the use of the optical flow method.[35,36] Furthermore, the directional error decreased with the flow rate, as shown in Fig. 7. The clutter filter used in the present study could suppress the signal components from objects that move with a velocity less than 0.1 m/s along a scan line. The average flow velocity along the flow axis was estimated to be 0.41 m/s from the flow rate at a rotation rate of 360/min and that along the scan line was also estimated to be 0.11 m/s (over 0.1 m/s corresponding the cutoff velocity) from the angle between the array surface and the tube. The directional error, therefore, would have been reduced because the SNRs of filtered signal slightly increased with a flow rate under the experimental conditions used.

7. Conclusions

In this study, high-frame-rate echocardiography with spherically diverging waves was used to continuously visualize echo speckles of blood particles. Coded excitation using the 13-bit Barker code and clutter filtering were also used to increase the SNR of weak echoes from blood particles. Moreover, the magnitude of the filtered RF signal was weighted by coherence to suppress the random noise remaining after clutter filtering. In the proposed method, magnitude compounding among transmissions was employed to obtain echo speckles with higher SNRs because echo signals from moving blood particles cancel each other when RF signals were compounded. The flow velocity vector was estimated by applying the speckle tracking technique to the visualized blood echo speckle. From the basic experimental result, the accuracy of the estimation of the velocity vector was improved by magnitude compounding. B-mode images overlaid with echo speckles of blood particles were obtained in the three-chamber view through in vivo measurement of a 26-year-old healthy male. Furthermore, the velocity vectors of blood flow could be visualized inside the left ventricular cavity by estimating the motion of echoes from blood particles between successive frames. The in vivo experimental results showed the feasibility of the noninvasive imaging of cardiac blood flow patterns using our proposed method.

Acknowledgments

This work was supported by JSPS Research Fellowships and the International Advanced Research and Education Organization of Tohoku University.

1) H. Kanai, Ultrasound Med. Biol. **35**, 936 (2009).
2) H. Shida, H. Hasegawa, and H. Kanai, Jpn. J. Appl. Phys. **51**, 07GF05 (2012).
3) E. Konofagou, J. Luo, K. Fujikura, D. Cervantes, and J. Coromilas, Proc. IEEE Ultrasonics Symp., 2006, p. 985.
4) M. Tanaka, T. Sakamoto, S. Sugawara, H. Nakajima, Y. Katahira, S. Ohtsuki, and H. Kanai, J. Cardiol. **52**, 86 (2008).
5) J. Luo and E. Konofagou, Ultrasound Med. Biol. **37**, 980 (2011).
6) G. R. Hong, G. Pedrizzentti, G. Tonti, P. Li, Z. Wei, J. K. Kim, A. Baweja, S. Liu, N. Chung, H. Houle, J. Narula, and M. A. Vannan, J. Am. Coll. Cardiol. Imaging **1**, 705 (2008).
7) R. Faludi, M. Szulik, J. D'hooge, P. Herijgers, F. Rademakers, G. Pedrizzetti, and J. U. Voigt, J. Thorac. Cardiovasc. Surg. **139**, 1501 (2010).
8) A. Kheradvar, H. Houle, G. Pedrizzetti, G. Tonti, T. Belcik, M. Ashraf, J. R. Lindner, M. Gharib, and D. Sahn, J. Am. Soc. Echocardiogr. **23**, 86 (2010).
9) P. Tortoli, G. Bambi, and S. Ricci, IEEE Trans. Ultrason. Ferroelectr. Freq. Control **53**, 1425 (2006).
10) P. Tortoli, A. Dallai, E. Boni, L. Francalanci, and S. Ricci, Ultrasound Med. Biol. **36**, 488 (2010).
11) J. A. Jensen and S. I. Nikolov, IEEE Trans. Ultrason. Ferroelectr. Freq. Control **51**, 1107 (2004).
12) M. Tanter, J. Bercoff, L. Sandrin, and M. Fink, IEEE Trans. Ultrason. Ferroelectr. Freq. Control **49**, 1363 (2002).
13) H. Hasegawa and H. Kanai, IEEE Trans. Ultrason. Ferroelectr. Freq. Control **55**, 2626 (2008).
14) J. Udesen, F. Gran, K. L. Hansen, J. A. Jensen, C. Thomsen, and M. B. Nielsen, IEEE Trans. Ultrason. Ferroelectr. Freq. Control **55**, 1729 (2008).
15) H. Hasegawa and H. Kanai, Proc. IEEE Ultrasonics Symp., 2010, p. 1319.
16) B. Y. S. Yiu and A. C. H. Yu, Ultrasound Med. Biol. **39**, 1015 (2013).
17) L. Lovstakken, S. A. Nyrnes, B. O. Haugen, and H. Torp, Proc. IEEE Ultrasonics Symp., 2011, p. 1246.
18) H. Hasegawa and H. Kanai, J. Med. Ultrason. **38**, 129 (2011).
19) H. Hasegawa and H. Kanai, IEEE Trans. Ultrason. Ferroelectr. Freq. Control **59**, 2569 (2012).
20) M. Karaman, P. C. Li, and M. O'Donnell, IEEE Trans. Ultrason. Ferroelectr. Freq. Control **42**, 429 (1995).
21) I. Akiyama, N. Yoshizumi, S. Saito, Y. Wada, D. Koyama, and K. Nakamura, Jpn. J. Appl. Phys. **51**, 07GF02 (2012).
22) A. Koriyama, W. Yasuhara, and H. Hachiya, Jpn. J. Appl. Phys. **51**, 07GF09 (2012).
23) G. E. Trahey, S. M. Hubbard, and O. T. von Ramm, Ultrasonics **26**, 271 (1988).
24) T. Higuchi, S. Hirata, T. Yamaguchi, and H. Hachiya, Jpn. J. Appl. Phys. **52**, 07HF19 (2013).
25) J. Ophir, I. Cespedes, H. Ponnekanti, Y. Yazdi, and X. Li, Ultrason. Imaging **13**, 111 (1991).
26) K. R. Nightingale, P. J. Kornguth, and G. E. Trahey, Ultrasound Med. Biol. **25**, 75 (1999).
27) R. K. Parajuli, R. Tei, D. Nakai, and Y. Yamakoshi, Jpn. J. Appl. Phys. **52**, 07HF22 (2013).
28) A. Tanaka and Y. Saijo, Proc. IEEE Engineering Medicine and Biology Society, 2007, p. 4500.
29) T. L. Szabo, *Diagnostic Ultrasound Imaging: Inside Out* (Academic Press, Waltham, MA, 2004) Chap. 8.2.
30) T. Sato, H. Tojo, and Y. Watanabe, Jpn. J. Appl. Phys. **52**, 07HF18 (2013).
31) R. Y. Chiao and X. Hao, IEEE Trans. Ultrason. Ferroelectr. Freq. Control **52**, 160 (2005).
32) M. R. Mahafza, *Introduction to Radar Analysis* (CRC Press, Boca Raton, FL, 1998) Chap. 6.11.
33) M. J. Garcia, L. Rodriquez, M. Ares, B. P. Griffin, A. L. Klein, W. J. Stewart, and J. D. Thomas, Am. Heart J. **132**, 648 (1996).
34) I. Cespedes, Y. Huang, J. Ophir, and S. Sprat, Ultrason. Imaging **17**, 142 (1995).
35) B. K. P. Horn and B. G. Schunck, Artif. Intell. **17**, 185 (1981).
36) I. Akiyama, Jpn. Med. Ultrason. **20**, 86 (1993).